Journal of Marine Research, 43, 493–516, 1985

Journal of
MARINE RESEARCH

Volume 43, Number 3

Western boundary circulation driven by an alongshore wind: With application to the Somali Current system

by Julian P. McCreary[1] and Pijush K. Kundu[1]

ABSTRACT

The linear, continuously stratified, eastern-boundary model of McCreary (1981) is extended to apply to a western ocean boundary and to wind fields with curl. The model has vertical and horizontal mixing, and both types of mixing are important in its dynamics. Solutions are represented as expansions in vertical modes, and the dynamics of low-order and high-order modes are very different. Low-order modes tend to be in Sverdrup balance in the interior ocean, and to form a Munk layer at the coast. High-order modes are in Ekman balance in the interior ocean, and the coastal balance is two dimensional.

The model is forced by steady northward winds, both with and without curl. Solutions at the western boundary differ fundamentally from comparable ones at the eastern boundary. For winds without curl, the surface jet is stronger, and there is essentially no coastal undercurrent. This difference is due to the fact that at an eastern boundary the currents associated with low-order modes leak offshore. For winds with curl, a sizeable undercurrent develops, but only south of the region of the wind. A strong onshore current, located near the southern edge of the wind, is generated by offshore wind curl. Part of this current turns southward at the coast, thereby generating the undercurrent in the south.

The existence of this undercurrent is in accord with observations off Somalia, where a southward undercurrent has been observed at 5N during the Southwest Monsoon. The wind at this time is oriented alongshore, reaches maximum strength well to the north of 5N, and is associated with a region of large, negative wind curl off the coast.

1. Introduction

The coastal circulation driven by an alongshore wind field has been studied extensively near the eastern boundary of an ocean. In contrast, there have been

1. Nova University, Oceanographic Center, 8000 North Ocean Drive, Dania, Florida, 33004, U.S.A.

relatively few studies of the corresponding flow near a western ocean boundary. One purpose of this study is to model such flows, and to contrast solutions with those near an eastern boundary. Another purpose is to relate solutions to observations of currents off the coast of Somalia, where the circulation is well known to be forced significantly by the alongshore wind field.

a. Observational background. Measurements in several parts of the world ocean have established what one might call a "classic upwelling regime" along an eastern ocean boundary. An equatorward wind drives an offshore surface flow, thereby inducing upwelling at the coast and a subsurface onshore flow. There is an equatorward surface jet and a poleward undercurrent at depths of 100–300 m that decay offshore with a scale of the order of 20–30 km. Both the transverse and alongshore circulations are surface-trapped features which do not extend to the ocean bottom. Isopycnals bend sharply upward toward the coast above the undercurrent core, indicating the occurrence of upwelling. Below the core they bend downward, indicating that the upwelling is surface trapped.

One western-boundary upwelling region that has been studied extensively is the coast of Somalia (see the recent review articles by Schott, 1983, and by Knox and Anderson, 1985). The alongshore winds there can be very strong (~5 dyn/cm^2), and they reverse direction seasonally with the monsoons. In response, the Somali Current also reverses seasonally. Soon after the onset of the Southwest Monsoon, a coastal circulation rather like that at an eastern boundary, but more intense, exists north of 5N. Cold water appears all along the coast of Somalia, although it is concentrated in wedges (Brown *et al.*, 1980). The surface poleward flow is very strong (~100–200 cm/s), and forms one or two quasi-stationary eddies (Düing *et al.*, 1980). There is an undercurrent with an instantaneous maximum speed as large as 60 cm/s (Leetmaa *et al.*, 1982), although the monthly average speed (Fig. 1a) has a maximum of only about 20 cm/s (Quadfasel and Schott, 1983; Schott and Quadfasel, 1982). The width scale of both currents is of the order of 50–100 km. The wind at this time is in the form of an alongshore jet which reaches a maximum speed near 10–15N (Fig. 1b), well north of the region of the undercurrent measurements (Luther and O'Brien, 1985; Knox and Anderson, 1985). Because of the jet-like structure of this wind, there is an offshore negative curl of about -5×10^{-8} dyn/cm^3 (Schott, 1983).

b. Theoretical background. McCreary (1981) studied eastern-boundary, upwelling circulation using a three-dimensional, continuously stratified model forced by a curl-free alongshore wind. Vertical diffusion of heat and momentum is an essential element in the dynamics of this model. The establishment of a baroclinic, alongshore pressure gradient field (via the radiation of Kelvin and Rossby waves) is also crucial. In agreement with observations, the resulting flow field was surface trapped with an equatorward surface jet and a poleward undercurrent (Fig. 2).

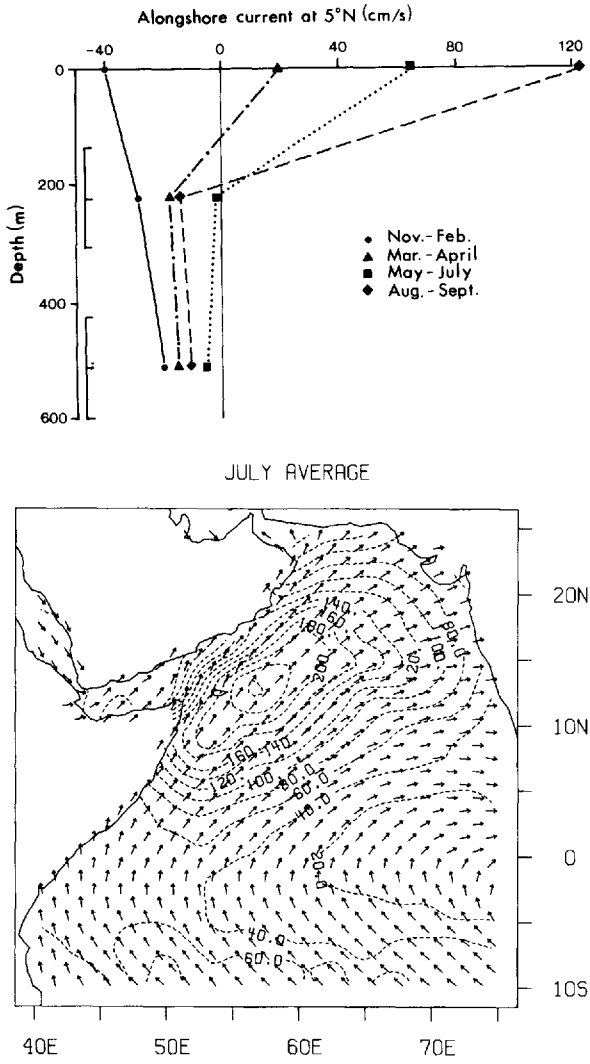

Figure 1. (a) Average alongshore current at 5N observed during 1975–1979, at a station about 50 km offshore. [Reproduced from Quadfasel and Schott, 1983.] (b) Wind pseudo-stress vector, defined as $\mathbf{V}|\mathbf{V}|$, averaged for the month of July. Contour interval is 20 $m^2 s^{-2}$, and the arrows represent direction only. The data are compiled from surface observations from 60 years of ship reports. [Reproduced from Luther and O'Brien, 1985.]

Previous theoretical work on the Somali Current system has been primarily concerned with the causes of the rapid response of surface currents to the changing winds, attempting to answer questions such as whether these currents are locally or remotely forced. Several of these studies use nonlinear, reduced-gravity models with a simple vertical structure (Anderson and Rowlands, 1976; Anderson and Moore, 1979;

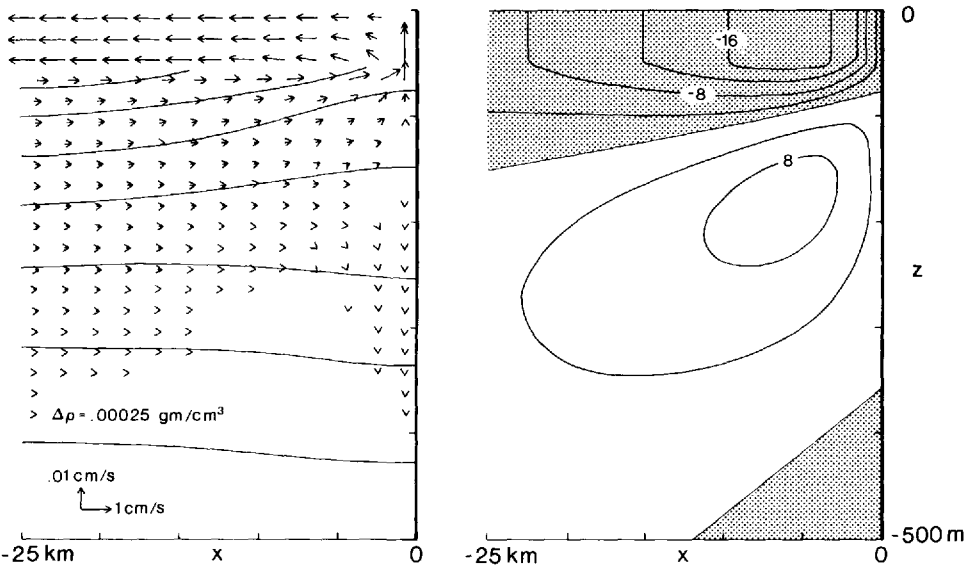

Figure 2. Zonal section at 35N of flow field near an eastern boundary driven by curl-free southward wind. The left panel shows transverse circulation and isopycnal structure, and the right panel shows alongshore currents. Calibration arrows are $(u, w) = (1., .01)$ cm/s and the contour intervals for density and velocity are .00025 gm/cm^3 and 4 cm/s, respectively. Regions of southward (negative) flow are shaded. Diffusivities are $\nu_{min} = 10$ cm^2/s and $\nu_h = 10^5$ cm/s. [After McCreary (1981).]

Lin and Hurlburt, 1981; Luther and O'Brien, 1985). Others use comprehensive general circulation models (Cox, 1976, 1979; Philander and Delecluse, 1983). These models point out various nonlinear aspects of the surface circulation; for example, solutions characteristically form eddies during spin-up and develop an inertial overshoot of coastal jets across the equator. There is little discussion of the vertical structure of coastal currents in any of these studies.

c. Present approach. The present study examines the generation of western boundary currents by steady alongshore winds. Other mechanisms of forcing western boundary currents, such as basin-wide wind curl and thermohaline driving, are not considered. So, our solutions are most relevant to the Somali Current system, since forcing by the alongshore wind is very strong there. The vertical structure of the currents, including the question of the generation of a coastal undercurrent, receives special attention.

The linear, continuously stratified, eastern-boundary model of McCreary (1981) is modified to apply to the western boundary, and is generalized to include wind curl. A simplifying assumption is that the alongshore current is in geostrophic balance, a restriction that prevents solutions from being applicable at the equator. The model involves both vertical and horizontal mixing, and both types are important in its

dynamics. Solutions have properties in common with those of simpler models (see the discussions in Section 2c and in the Appendix). These similarities provide a useful way of discussing its dynamics.

Important results are the following. A wind without curl does *not* generate a coastal undercurrent, in contrast to the solution in Figure 2. A wind with offshore curl, however, does develop an undercurrent, but only south of the wind. This undercurrent exists for a very different reason than the one at the eastern boundary. A strong onshore current, located at the southern edge of the wind, is remotely forced by offshore wind curl; part of this current bends to the south at the coast, thereby generating the undercurrent. The existence of this undercurrent is consistent with the observations of the Somali Current discussed above.

An obvious limitation of the model is that it is linear, and it is well known that nonlinearities do affect western boundary currents. Nevertheless, we feel that the solutions found here are useful for several reasons. First, nonlinear terms often act simply to modify linear solutions, rather than to change them completely; compare, for example, the linear and nonlinear calculations given in Philander and Delecluse (1983). Second, the subsurface currents, which are of primary interest here, are considerably weaker than the surface currents, and therefore may be less affected by nonlinearities. Third, numerical models typically have limited vertical resolution, which may not be adequate to study the subsurface current structures; in contrast, the vertical resolution of the present analytical model is virtually unlimited. Finally, and perhaps most importantly, the dynamics of linear solutions are certainly also involved in those of nonlinear solutions in a fundamental way. We therefore expect that the solutions found here will provide insights into the understanding of more sophisticated models and the observed currents themselves.

2. The model ocean

a. Equations and boundary conditions. The equations of motion are linearized about a state of rest with a density field $\rho_b(z)$ and associated buoyancy frequency $N_b(z)$. The distribution $\rho_b(z)$ must have a surface mixed layer of thickness h in which $N_b = 0$, but can have any stably stratified profile in the deeper ocean. The model is forced by an oscillating meridional wind stress $\tau^y(x, y)\, e^{i\sigma t}$; however, in this paper we discuss only steady solutions with $\sigma = 0$. Equations for the amplitudes of the flow variables are

$$\begin{aligned} -fv + p_x &= 0, \\ i\sigma v + fu + p_y &= (\nu v_z)_z + \nu_h v_{xx}, \\ i\sigma\rho - N_b^2 w/g &= (\nu\rho)_{zz} + \nu_h \rho_{xx}, \\ p_z &= -\rho g, \\ u_x + v_y + w_z &= 0. \end{aligned} \tag{1}$$

The coordinates x, y and z and the velocity amplitudes u, v, and w are directed eastward, northward and upward, respectively. The pressure and density changes from

the background state are p and ρ. The Coriolis parameter is $f = 2\Omega \sin(y/R)$, where $\Omega = 2\pi$ day^{-1} and R is the radius of the earth. Horizontal and vertical mixing coefficients are ν_h and ν respectively, and $\nu = A/N_b^2$. The mixing coefficients of heat and momentum are assumed equal for convenience, although the model can be easily generalized to non-unit Prandtl numbers.

Boundary conditions at the ocean surface are

$$w = \nu\rho = 0, \nu v_z = \tau^y \qquad \text{at } z = 0, \tag{2a}$$

and at the flat ocean bottom are

$$w = \nu\rho = \nu v_z = 0 \qquad \text{at } z = -D. \tag{2b}$$

No-slip conditions are adopted at meridional boundaries, so that

$$u = v = 0 \qquad \text{at } x = x_B. \tag{3}$$

Finally, the solutions must remain bounded in the far field.

These equations and boundary conditions involve several assumptions that are special to the method of solution used here. First, the alongshore flow is in geostrophic balance, which is a good assumption for low-frequency flows outside the equatorial Rossby radius (~2°–4° of latitude). Second, the Laplacian operator is replaced by ∂_{xx} in the horizontal-mixing terms. These two assumptions ensure that the equation for p alone does not involve y-derivatives, as in (9) below. Third, the vertical mixing coefficients are inversely proportional to N_b^2 and the mixing of heat has the form $(\nu\rho)_{zz}$. Fourth, the surface and bottom values of $\nu\rho$ and the bottom stress are fixed to be zero. These two assumptions ensure that solutions can be represented as expansions in the vertical normal modes of the system, as in Eqs. (4).

A final requirement is that the model has a surface mixed layer where $N_b = 0$. Physically, the reason for this requirement is that the restriction of alongshore geostrophy filters Ekman layers out of the model [see the discussion of (A1) in the Appendix]. Thus, the mixed layer is necessary in order to be able to introduce stress into the ocean. Mathematically, the reason is that without the mixed layer the normal-mode expansions do not converge. For example, the lack of convergence is evident for the Ekman and Sverdrup flows produced by the model [defined below in (11) and (25) respectively], for which the surface flows are inversely proportional to the thickness of the mixed layer, h.

The normal-mode expansions are

$$(u, v, p) = \sum_{n=0}^{N} (u_n, v_n, p_n)\psi_n, \quad w = \sum_{n=0}^{N} w_n\psi_{nz}, \quad \rho = \sum_{n=0}^{N} \rho_n \int_{-D}^{z} \psi_n dz, \tag{4}$$

where the functions $\psi_n(z)$ satisfy

$$\psi_{nz} = -\frac{N_b^2}{c_n^2} \int_{-D}^{z} \psi_n dz, \tag{5}$$

subject to the constraint

$$\frac{1}{c_n^2}\int_{-D}^{0}\psi_n\,dz = 0, \tag{6}$$

and the eigenvalues c_n are the characteristic speeds associated with each mode. The modes are normalized here so that $\psi_n(0) = 1$. In principle, the sums in (4) extend from $n = 0$ to ∞; in practice, they are necessarily truncated at a finite number of terms N.

The expansion coefficients satisfy the equations

$$\begin{aligned} -f v_n + p_{nx} &= 0,\\ \omega v_n + f u_n + p_{ny} &= G_n + \nu_h v_{nxx},\\ \omega p_n + c_n^2(u_{nx} + v_{ny}) &= \nu_h p_{nxx},\\ c_n^2 w_n &= \omega p_n + \nu_h p_{nxx},\\ \rho_n &= -p_n/g, \end{aligned} \tag{7}$$

where $\omega = i\sigma + A/c_n^2$, and

$$G_n = \frac{\tau^y}{\int_{-D}^{0}\psi_n^2\,dz}\,. \tag{8}$$

Note that vertical mixing affects each mode as a simple drag with a drag coefficient A/c_n^2. Because c_n decreases with modenumber roughly like n^{-1}, higher-order modes are strongly damped.

b. The solution. An equation for p_n alone derived from (7) is

$$\nu_h p_{nxxxx} - \omega p_{nxx} - \nu_h \alpha^2 p_{nxx} - \beta p_{nx} + \omega\alpha^2 p_n = -fG_{nx} \tag{9}$$

where $\alpha^{-1} = c_n/f$ is the Rossby radius and $\beta = f_y$. The method of solution is to solve (9) for p_n; Eqs. (7) are then used to solve for u_n, v_n, ρ_n and w_n in terms of p_n. Finally, the complete solution is determined by numerically evaluating the sums in (4).

Solutions to (9) can be conveniently written down as the sum of two pieces: an unbounded solution (designated by primed variables) and a boundary contribution (designated by double-primed variables). The unbounded solution is the response to τ^y when there is no coastal boundary at $x = x_B$. The boundary contribution is a solution to the unforced version of (9) which ensures that the total flow field satisfies the boundary conditions (3). To be explicit, we look for solutions to (9) of the form $p_n = p_n' + p_n''$, such that $u_n' + u_n'' = 0$ and $v_n' + v_n'' = 0$ at $x = x_B$.

i. Unbounded solutions

For convenience, the horizontal structure of the wind amplitude is assumed to have the separable form

$$\tau^y = \tau_o X(x) Y(y). \tag{10}$$

The function $Y(y)$ is meridionally bounded with both its northern and southern edges being north of the equator. For winds without curl, $X(x) = 1$. For winds with curl, $X(x)$ is assumed to be zonally bounded with eastern and/or western edges.

When the wind has no curl ($G_{nx} = 0$) the unbounded solution to (9) is simply $p'_n = 0$. It follows that the complete solution is

$$u'_n = G_n/f, \quad v'_n = w'_n = p'_n = \rho'_n = 0. \tag{11}$$

Because these coefficients do not involve c_n, it is possible to evaluate the sums (4) analytically. The resulting solution is a slab-like Ekman drift, $u' = \tau^y/fh$, confined entirely to the surface mixed layer. For this reason, we refer to a particular vertical mode with the expansion coefficients (11) as being in Ekman balance.

The unbounded solution is more complicated when the wind has curl ($G_{nx} \neq 0$). Let $\tilde{p}_n$ denote the zonal Fourier transform of p_n, that is, $\tilde{p}_n(k) = \int_{-\infty}^{\infty} p_n(x)e^{-ikx}dx$. Similarly, let G_{nx} have the Fourier transform $\tilde{G}_{nx}$, which does exist since the wind field is zonally bounded. The transform of (9) is then

$$[\nu_h k^4 + (\omega + \alpha^2\nu_h)k^2 - i\beta k + \omega\alpha^2]\tilde{p}'_n = -f\tilde{G}_{nx}. \tag{12}$$

Let k_j ($j = 1, 2, 3, 4$) be the roots of

$$k_j^4 + \left(\frac{\omega}{\nu_h} + \alpha^2\right)k_j^2 - \frac{i\beta}{\nu_h}k_j + \frac{\omega\alpha^2}{\nu_h} = 0. \tag{13}$$

Then (12) can be written as

$$\tilde{p}'_n = -\frac{f\tilde{G}_{nx}/\nu_h}{\prod_{j=1}^{4}(k - k_j)}, \tag{14}$$

and the expansion of (14) into partial fractions yields

$$\tilde{p}'_n = -\frac{f\tilde{G}_{nx}}{\nu_h}\sum_{j=1}^{4}\frac{1}{(k - k_j)(k_j - k_{j'})(k_j - k_{j''})(k_j - k_{j'''})} \tag{15}$$

where $k_{j'}$, $k_{j''}$ and $k_{j'''}$ are the three roots of (13) that are different from k_j. Finally, the inverse transform of (15) gives the desired solution

$$p'_n = -\frac{if}{\nu_h}\sum_{j=1}^{4}\frac{e^{ik_jx}\int_{Lj}^{x} e^{-ik_jx}\,G_{nx}\,dx}{(k_j - k_{j'})(k_j - k_{j''})(k_j - k_{j'''})}. \tag{16}$$

The other field variables can now be found from (7) using (16).

The integrals in (16) involve the choices of lower limits L_j. Two of the roots (labelled k_1 and k_2) have a negative imaginary part, and two of them (labelled k_3 and k_4) have a positive imaginary part. Then the choices $L_1 = L_2 = +\infty$ and $L_3 = L_4 = -\infty$ ensure that p'_n remains finite as $x \longrightarrow \pm\infty$.

Because the wind has the separable form (10), the complete forced solution can be written in the compact form

$$\begin{aligned}
p'_n &= -\frac{if\tau_n Y}{\nu_h}\sum_{j=1}^{4}\frac{Q_j}{S_j},\\
u'_n &= \frac{G_n}{f}+\frac{\tau_n Y}{\nu_h f}\sum_{j=1}^{4}\left[i\left(\beta+\frac{fY_y}{Y}\right)-ifR_j-\omega k_j-\nu_h k_j^3-if\frac{Q_{jy}}{Q_j}\right]\frac{Q_j}{S_j},\\
v'_n &= \frac{\tau_n Y}{\nu_h}\sum_{j=1}^{4}\frac{k_j Q_j}{S_j},\\
w'_n &= -\frac{if\tau_n Y}{c_n^2}\sum_{j=1}^{4}\left(\frac{\omega}{\nu_h}+k_j^2\right)\frac{Q_j}{S_j},\\
\rho'_n &= -p'_n/g,
\end{aligned} \tag{17}$$

where

$$\begin{aligned}
Q_j(x,y) &= e^{ik_j x}\int_{Lj}^{x} e^{-ik_j x}X_x dx,\\
S_j(y) &= (k_j-k_{j'})(k_j-k_{j''})(k_j-k_{j'''}),\\
R_j(y) &= (\ln S_j)_y,
\end{aligned} \tag{18}$$

and $\tau_n = \tau_o/\int_{-D}^{0}\psi_n^2\,dz$. Analytical expressions for Q_j can be found for the choices of $X(x)$ used in this paper.

ii. Boundary contribution

The contributions due to the presence of the boundaries are free solutions of the form $P_j \exp[ik_j(x - x_B)]$; these solutions satisfy (9) without the wind-forcing term. Consider first the effect of a western boundary at $x = x_W$. The boundary contribution is

$$\begin{aligned}
p''_n &= \sum_{j=3}^{4}P_j e^{ik_j(x-x_W)},\\
u''_n &= -\frac{1}{f}\sum_{j=3}^{4}(i\omega k_j+i\nu_h k_j^3+f\partial_y)P_j e^{ik_j(x-x_W)},\\
v''_n &= \frac{i}{f}\sum_{j=3}^{4}k_j P_j e^{ik_j(x-x_W)}.
\end{aligned} \tag{19}$$

The sums are only for $j = 3$ and 4, since the solution must include only exponentials that decay eastward from the western boundary.

The functions $P_j(y)$ are determined by imposing the boundary conditions $u'_n + u''_n = v'_n + v''_n = 0$ at $x = x_W$, and are

$$\begin{aligned}
P_3 &= \frac{k_4}{k_4-k_3}e^{\Lambda}\int_L^y e^{-\Lambda}g_n\,dy,\\
P_4 &= \frac{if}{k_4}v'_W-\frac{k_3}{k_4}P_3,
\end{aligned} \tag{20}$$

where

$$\Lambda = i\nu_h \int^y \frac{k_3 k_4}{f}(k_3 + k_4)\, dy',$$
$$g_n = fu'_W + v'_W\left(\omega + \nu_h k_4^2 - \frac{i\beta}{k_4} + \frac{ifk_{4y}}{k_4^2}\right) - \frac{if}{k_4} v'_{Wy}, \tag{21}$$

and u'_W and v'_W are the contributions of the unbounded solutions, (11) or (17), at the boundary. The lower limit L of the y-integration in (20) is any point poleward of the wind band. Any other choice for L generates a boundary current that grows exponentially to the north, which is not allowed since the solution must remain bounded in the far field. The lower limit of the y-integration in (21) is arbitrary.

The offshore and meridional structures of the boundary currents are evident in (19) and (20). Because P_3 is proportional to an integral of g_n, rather than to g_n itself, P_3 does not vanish equatorward of the wind. Instead, it is proportional to e^{Λ} there, and decays equatorward with an alongshore decay scale l^{-1}, where

$$l \equiv (e^{\Lambda})_y / e^{\Lambda} = \Lambda_y = \frac{i\nu_h}{f} k_3 k_4 (k_3 + k_4). \tag{22}$$

Provided that l^{-1} is sufficiently large, boundary currents extend well south of the wind. A measure of the offshore decay scale of the flow is the larger of $|k_3|^{-1}$ and $|k_4|^{-1}$.

The boundary contribution due to an eastern wall at $x = x_E$ can be found similarly. The solution there is the same as (19) – (21) except that (x_W, u'_W, v'_W) are replaced by (x_E, u'_E, v'_E), the lower limit L is a point equatorward of the wind band, and the sums are for $j = 1, 2$ so that exponentials decay westward from the boundary.

c. Dynamics. Recall that c_n decreases with modenumber roughly like n^{-1}. A consequence of this decrease is that the steady-state ($\sigma = 0$) response of the low-order modes is very different from that of the high-order modes (McCreary, 1981). To illustrate the differences, it is useful to consider properties of the solutions in the limits $c_n \to \infty$ and $c_n \to 0$. In these limits the solutions simplify considerably to familiar forms.

When $c_n \to \infty$ all the mixing terms in (7) except the term $\nu_h \nu_{nxx}$ are negligible. The resulting set of equations is essentially the same as the set solved by Munk (1950). Provided that the horizontal scale of the wind is considerably larger than $(\nu_h/\beta)^{1/3}$, the unbounded solution (17) is

$$u'_n = -\left(\frac{G_n}{\beta}\right)_y, \quad v'_n = \frac{G_{nx}}{\beta}, \quad w'_n = 0, \quad p'_n = \frac{fG_n}{\beta}, \tag{23}$$

a state of Sverdrup balance. The roots of (13) reduce to

$$ik_1 = \frac{\omega\alpha^2}{\beta} \to 0, \quad ik_2 = \left(\frac{\beta}{\nu_h}\right)^{1/3}, \quad ik_{3,4} = \frac{1}{2}(-1 \pm i\sqrt{3})\left(\frac{\beta}{\nu_h}\right)^{1/3}, \tag{24}$$

with ik_3 and ik_4 being complex conjugates, and it follows that $l^{-1} = f/\beta = R \tan(y/R) \approx y$. We will subsequently refer to a western boundary current with these values of k_3, k_4 and l as being a Munk layer. Since k_1 and k_2 differ from k_3 and k_4 the offshore structures of eastern and western boundary solutions are not the same. The fact that k_1 is small indicates that eastern boundary currents leak offshore by means of the radiation of long-wavelength Rossby waves (McCreary, 1981). Finally, $w_n = 0$ in this limit, and so there is no coastal upwelling. Instead, because the flow is horizontally non-divergent ($u_{nx} + v_{ny} = 0$), offshore (onshore) transport forced by the wind is necessarily balanced by a northward (southward) western boundary current to the south.

If all the modes of the unbounded solution are in Sverdrup balance, it is possible to evaluate the sums (4) analytically. The solutions are

$$u' = -\left(\frac{\tau^y}{h\beta}\right)_y = -\frac{\tau^y_y}{\beta h} + \frac{\beta_y \tau^y}{\beta^2 h},$$
$$v' = \frac{\tau^y_x}{\beta h}, \quad w' = 0, \quad p' = \frac{f\tau^y}{\beta h}, \tag{25}$$

a Sverdrup flow confined entirely to the mixed layer. Consider the Sverdrup flow generated by a northward wind stress patch like the one shown in Figure 4. Looking down from above, (25) represents a clockwise gyre with currents located primarily in the "cosine" edges of the wind patch; there is also a weak westward flow in the region of uniform wind due to the term proportional to β_y in (25). Note that the pressure field is also located completely inside the region of the wind patch.

When $c_n \to 0$ the vertical mixing terms dominate the balances in (7) and the terms p_{ny} and v_{ny} are negligible. The balance of terms is therefore a two-dimensional one. The unbounded solution (17) is just the solution (11), a state of Ekman balance. The roots of (13) reduce to

$$ik_1 = \alpha, \quad ik_2 = \left(\frac{\omega}{\nu_h}\right)^{1/2}, \quad ik_3 = -\alpha, \quad ik_4 = -\left(\frac{\omega}{\nu_h}\right)^{1/2}, \tag{26}$$

with ik_3 and ik_4 being real, and $l^{-1} = c_n/\omega \to 0$. Since $k_1 = -k_3$ and $k_2 = -k_4$, the offshore structures of eastern and western boundary currents are *identical*. Because the flow field is two dimensional ($u_{nx} + w_{nz} = 0$), offshore transport forced by the wind is balanced by upwelling, rather than by the generation of an alongshore current.

For the choices of parameters used here, a few low-order modes ($n \lesssim 5 - 10$) tend toward the balances characterized by the limit $c_n \to \infty$. For these modes $|k_1|^{-1}$ is much larger than the zonal scale of the wind, ik_3 and ik_4 are complex conjugates, and $l^{-1} \approx y$. Contributions from these modes superpose to generate strong horizontal currents. The high-order modes are essentially in two-dimensional balance. For these modes $|k_j|^{-1}$ is much smaller than the zonal scale of the wind for all j, ik_3 and ik_4 are real, and $l^{-1} \ll y$. They superpose to generate Ekman drift in the interior ocean and coastal upwelling.

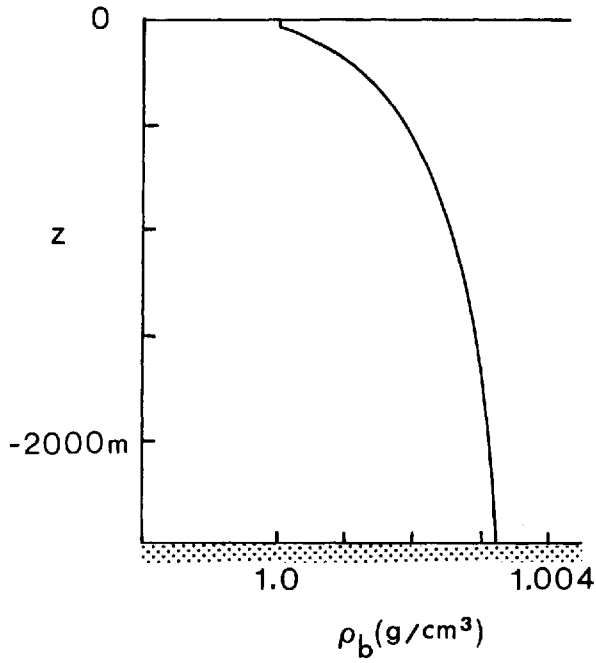

Figure 3. Background density distribution used for all the solutions shown in this paper.

3. Results

a. Choice of parameters. Figure 3 shows the background density profile generally used for all the solutions shown in this paper. It is the same as the one used in McCreary (1981), and is typical for mid-latitude upwelling regions. The profile has a pycnocline with a maximum buoyancy frequency $N_{max} = 0.89 \times 10^{-2}s^{-1}$, and a surface mixed layer of thickness $h = 50$ m. The depth of the ocean is $D = 2500$ m. Unless stated otherwise, the horizontal diffusivity is taken to be $\nu_h = 10^5$ cm^2/s. The vertical diffusivity, $\nu = A/N_b^2$, varies with depth because of the variation of $N_b(z)$, and it is usually set so that its minimum value is $\nu_{min} = A/N_{max}^2 = 1$ cm^2/s. The effects of other density structures and other values of diffusivity are studied in a few runs.

Throughout the paper the wind stress is taken to be steady (so that $\sigma = 0$) and northward. Figure 4 illustrates the horizontal structure of the wind used for all solutions except the one in Figure 12. The meridional profile $Y(y)$ is constant between 25N and 35N, and drops smoothly to zero at 20N and 40N with cosine tapers. The zonal profile $X(x)$ varies, and is specified in each case. When the wind has zonal edges, they also have the structure of cosine tapers. The wind amplitude τ_o is .5 dyn/cm^2, except for the solution in Figure 12.

The sums (4) are carried over 100 vertical modes. This value for N is sufficiently large for solutions to be well converged.

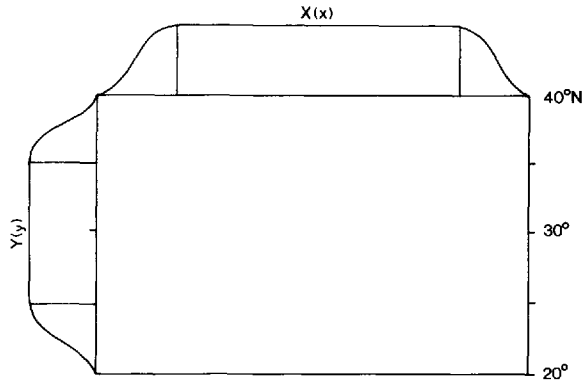

Figure 4. Zonal and meridional distributions of the wind. Edges of the wind drop smoothly to zero with cosine tapers.

b. Solutions without wind curl. Figure 5 shows the western-boundary solution forced by an x-independent wind. It shows a zonal section of the circulation at $y = 25$N, and it is comparable to the eastern-boundary solution of Figure 2. [The western-boundary solution at 25N and the eastern-boundary solution at 35N are equivalent locations with respect to the wind band because of the different directions of integration in (20).]

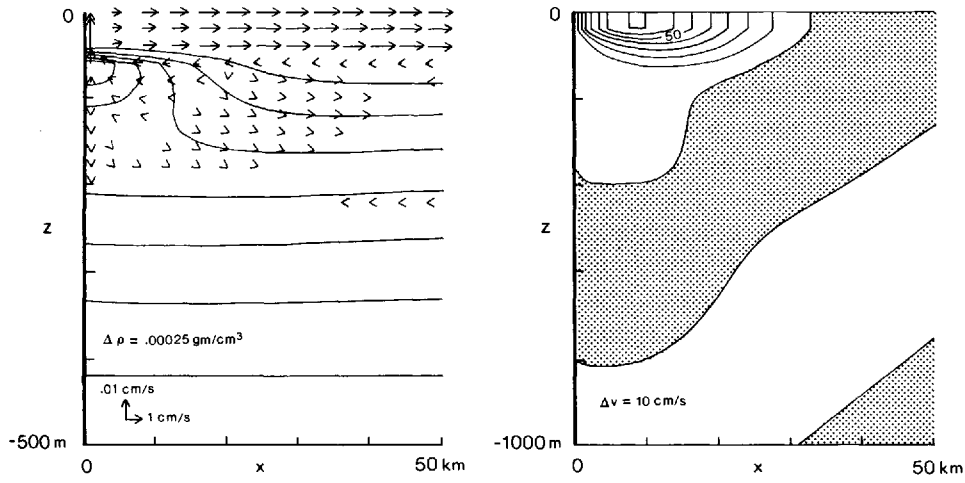

Figure 5. Zonal section at 25N of the flow field near a western boundary, driven by curl-free northward wind. The left panel shows transverse circulation and isopycnal structure in the upper 500 m with a contour interval of .00025 gm/cm^3. The right panel shows alongshore velocity in the upper 1000 m with a contour interval of 10 cm/s, and regions of southward (negative) flow are shaded. Diffusivities used are $\nu_{min} = 1$ cm^2/s, and $\nu_h = 10^5$ cm^2/s. Comparing with Figure 2, note that the western boundary current is stronger and has virtually no undercurrent.

The transverse circulations at the eastern and western boundaries are quite similar, but the alongshore flows are strikingly different. In particular, the surface flow along the western boundary is much stronger and there is *virtually no undercurrent.* Equatorward flow exists only at depths greater than 400 m, and is weaker than 0.16 cm/s. Note that there is a weak density inversion just beneath the surface mixed layer. It exists because of the linearization of the density equation in (1), and can be eliminated by increasing either ν or ν_h.

The reason for the similarity of the transverse circulations is that they are both dominated by contributions from high-order modes, for which the response at both boundaries is identical [see the discussion of Eqs. (26)]. The reason for the difference of the alongshore currents is that both are affected by low-order modes, for which the responses at the two boundaries differ markedly [see the discussion of Eqs. (24)]. At the eastern boundary, coastal currents associated with low-order modes leak offshore, and so do not contribute to the total circulation. No such process occurs at the western boundary, and contributions from low-order modes dominate the alongshore flow field there. The importance of β in causing the asymmetry is obvious, and the solutions at the two coasts are identical if $\beta = 0$.

The alongshore velocity distribution at the surface in Figure 5 resembles that of a Munk layer. According to (24), this structure is

$$v = v_o\, e^{-l_M x/\sqrt{3}} \sin(l_M x), \quad l_M = \frac{\sqrt{3}}{2}\left(\frac{\beta}{\nu_h}\right)^{1/3}. \tag{27}$$

With the assumed value of $\nu_h = 10^5$ cm^2/s, a countercurrent exists for $x > 30$ km, in agreement with Figure 5. The distribution with depth, however, indicates that the boundary current is not exactly a Munk layer. Contours of v tilt westward with depth, a property that involves both vertical diffusion and β (see the discussion in the Appendix).

Figure 6 shows the alongshore velocity and pressure gradient p_y along a meridional plane at a distance of $x = 8$ km from the coast, the distance at which v reaches its maximum value in Figure 5. (The pressure distribution along the coast was found to be very similar to that at $x = 8$ km.) Note that there is a strong poleward surface current south of the wind, but that there is never a significant undercurrent anywhere along the coast. The variation of sea level is also shown above the plot of p_y, and is similar to that at the eastern boundary (McCreary, 1981). An equatorward pressure gradient exists in the region of the wind down to a depth of 200 m, but it is *not* accompanied by an equatorward undercurrent.

The effect of varying vertical diffusivity is shown in Figure 7. A reduction of vertical diffusion not only increases the strength of the surface current, but also decreases the westward tilt of the v-contours with depth, a property that is consistent with the solution in the Appendix. Figure 7 also shows that the surface-layer structure does not resemble that of the Munk layer in the presence of high vertical diffusivities. For

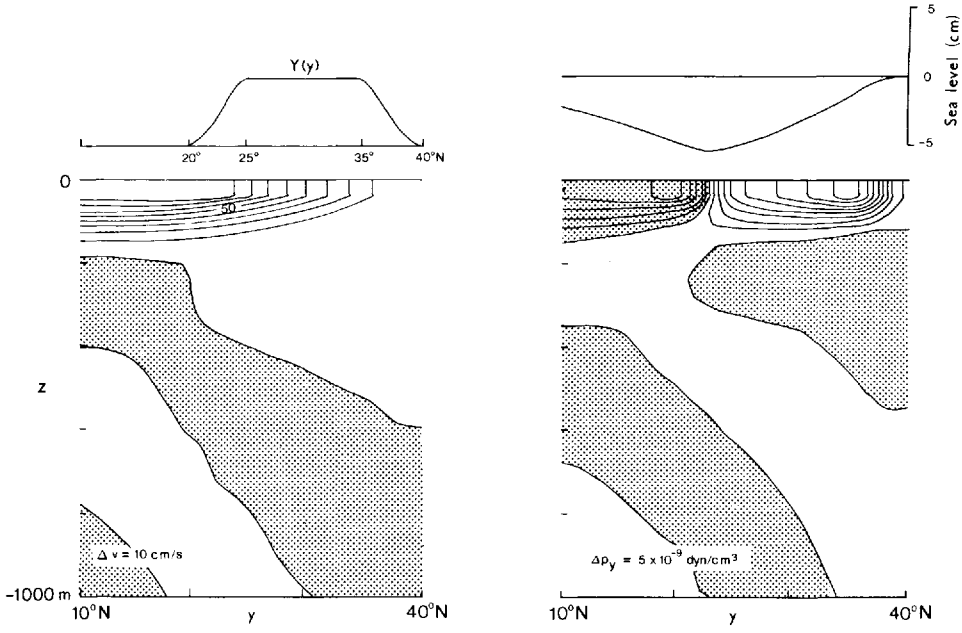

Figure 6. Meridional section of the flow field driven by a curl-free alongshore wind, at $x = 8$ km from western boundary. The left panel shows alongshore velocity, with a contour interval of 10 cm/s. The right panel shows pressure gradient p_y, with a contour interval of 5×10^{-9} dyn/cm^3. Regions of southward flow are shaded. Meridional distributions of the wind (upper left panel) and of sea level (upper right panel) are also indicated. Diffusivities used are $\nu_{min} = 1$ cm^2/s and $\nu_h = 10^5$ cm^2/s. Figure 5 shows a zonal section across this flow.

example, note that when $\nu_{min} = 100$ cm^2/s there is no countercurrent for $x > 30$ km. This difference is expected, since for sufficiently large values of ν the roots k_3 and k_4 are no longer complex conjugates, but rather are purely imaginary.

The effect of varying horizontal diffusivity was examined by finding solutions for $\nu_h = 10^4$ cm^2/s and 10^6 cm^2/s. The thickness of the coastal circulation increased like $\nu_h^{1/3}$, as expected for a Munk layer. The vertical penetration of the region of surface poleward flow was not affected much by these variations, and consequently the maximum surface velocity decreased as $\nu_h^{-1/3}$. (Also see the solution in Figure 12, for which $\nu_h = 10^7$ cm^2/s.)

To see the effect of varying the density stratification, the background density profile of Figure 3 was replaced by a linear profile with the same total change in density, but having a uniform value of $N_b = 0.36 \times 10^{-2}$s^{-1} below the mixed layer. The currents were found to be less surface trapped, and consequently smaller in magnitude. Another noticeable feature was that the ν-contours tilted downward to the west with a more uniform slope than in the previous figures. Other than these differences, the solutions with uniform stratification were qualitatively similar to those with a thermocline.

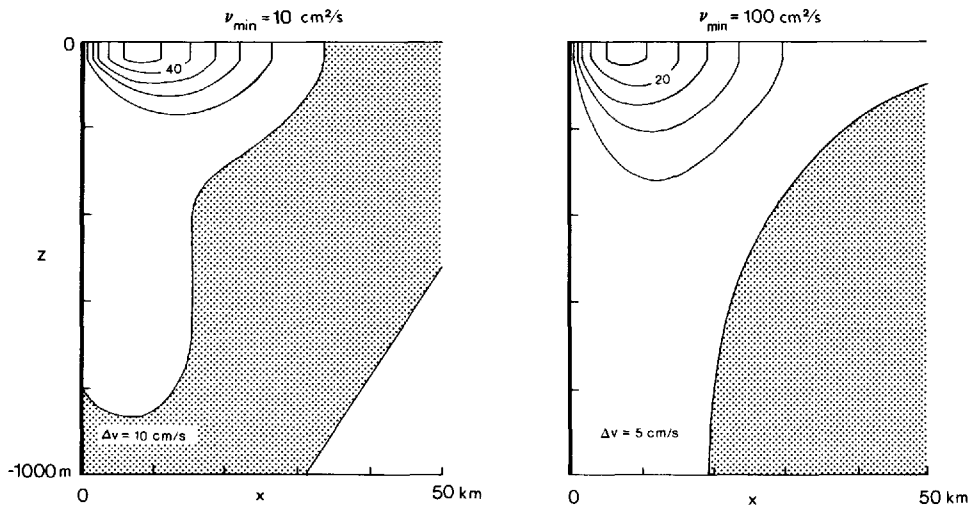

Figure 7. As in the right panel of Figure 5, except that ν_{min} = 10 cm^2/s and 100 cm^2/s in the left and right panels, respectively. These solutions should be compared to that in Figure 5, for which ν_{min} = 1 cm^2/s. As vertical mixing decreases the coastal current strengthens and shallows, and ν-contours slope less sharply into the deep ocean.

c. Solutions with wind curl. As discussed in Section 2b, the unbounded solution provides the forcing function for the coastal circulation. The solutions of the last section were forced by a wind without curl, and the interior solution was simply an Ekman drift. When there is wind curl, the interior flow is no longer just an Ekman drift, and this change has a significant effect on the resulting coastal circulation. We therefore begin this subsection by considering the effects of forcing by wind curl in an unbounded ocean.

i. Unbounded solution

Figure 8 shows the response of an unbounded ocean to a patch of northward wind τ^y, uniform in the middle and tapering off to zero along the edges (Fig. 4). The two upper panels show the circulation and pressure contours on a horizontal section at the surface, the bottom left panel shows ν-contours on a zonal section at 30N, and the bottom right panel shows u-contours on a meridional section at $x = 0$. The position of these sections, and the zonal and meridional distributions of the wind, are indicated in the top left panel.

Recall that the inviscid solution to (7) is a Sverdrup flow, (25), that is completely trapped in the surface mixed layer. The flow field in Figure 8 resembles a Sverdrup flow in that surface currents form a clockwise gyre largely confined to the edges of the wind, a consequence of the fact that the low-order modes tend toward Sverdrup balance. The circulation, however, differs from inviscid Sverdrup flow in several ways.

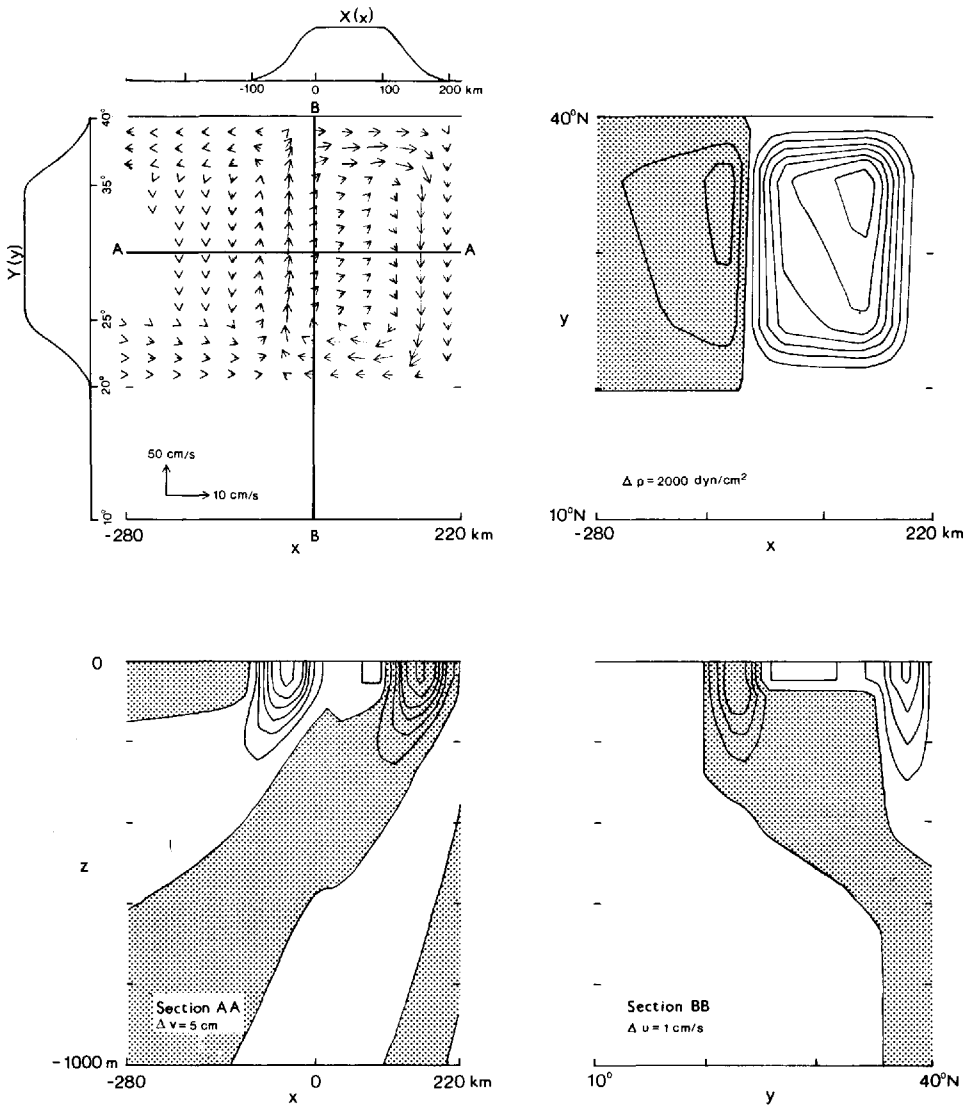

Figure 8. Unbounded flow driven by a patch of poleward wind with curl. Zonal and meridional distributions of the wind are shown alongside the upper left panel. The upper panels show circulation and p-contours on a horizontal section at the surface. The lower left panel shows v-contours on a zonal section at 30N, marked AA in top left panel. The bottom right panel shows u-contours on a meridional section at $x = 0$ km, marked BB. Regions of negative fields are shaded, and contour intervals are indicated in each panel. Diffusivities used are $\nu_{min} = 1\ \text{cm}^2/\text{s}$ and $\nu_h = 10^5\ \text{cm}^2/\text{s}$. The zonal flow in the lower right panel is the forcing function for the coastal currents in Figures 9–11.

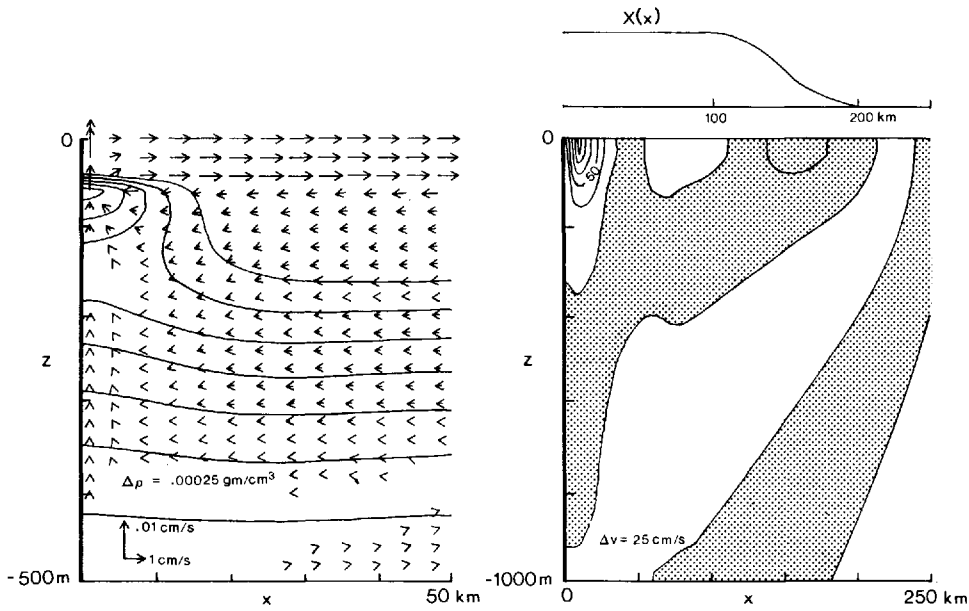

Figure 9. As in Figure 5, except driven by a northward wind with offshore curl. Note the different spatial scales of the two panels. The zonal distribution of wind is shown at the top of the right panel. The coastal current is considerably stronger than that in Figure 5.

First, the currents and pressure gradients are no longer confined to the surface mixed layer, and ν-contours now slope downward to the west, roughly according to (A3). Second, there is some leakage of surface currents and perturbation pressures west of the wind patch, a result of the westward propagation and decay of Rossby waves during the spin-up stage (McCreary, 1981). Third, in the region of uniform wind (latitude 25–35N), the surface flow is eastward ($u \sim 1$ cm/s), even though the depth-integrated (Sverdrup) transport at these latitudes is westward and equals $\int_{-D}^{0} u\, dz = +\beta_y \tau^y/\beta^2$. The reason for the eastward surface flow is that the high-order modes are not in Sverdrup balance, but rather are in Ekman balance.

ii. Bounded solutions

We now consider the effect of placing a boundary at the position $x = 0$ in Figure 8, that is, along section BB. The zonal flow along this section (lower righthand panel of Fig. 8) is the dominant forcing function for the coastal circulation, and the structure of the coastal currents are closely related to the structure of this forcing function.

Figures 9–11 show the resulting flow field. The zonal section at 25N (Fig. 9) shows an intensification of the boundary current ($v_{max} = 134$ cm/s) over the curl-free case of Figure 5 ($v_{max} = 71$ cm/s). This coastal intensification is caused by the strong offshore interior flow located at the northern edge of the wind (Fig. 8). There is a weak and

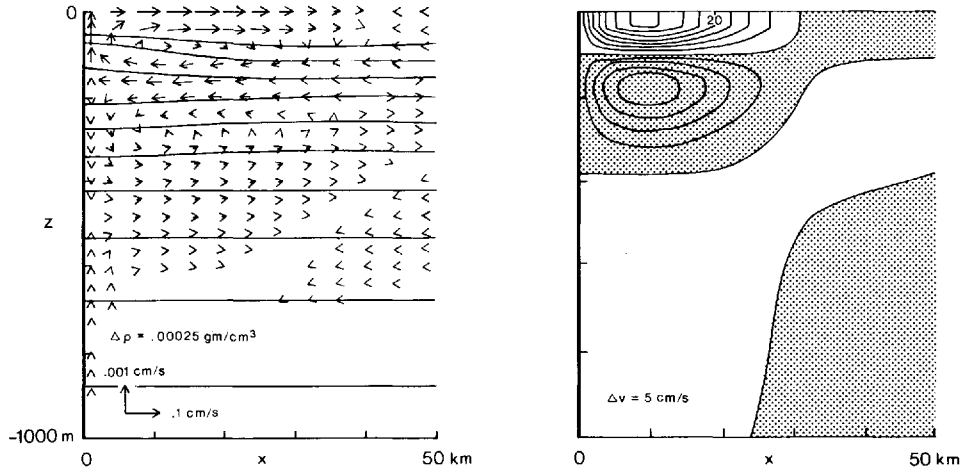

Figure 10. As in Figure 9, except at 10N. Note that the offshore extent of the right panel is 50 km, compared to 250 km in Figure 9. There is a coastal undercurrent reaching a maximum strength of $v = -23$ cm/s at a depth of 150 m. The undercurrent is forced by the region of strong onshore flow that is evident near 23N in the lower right panel of Figure 8.

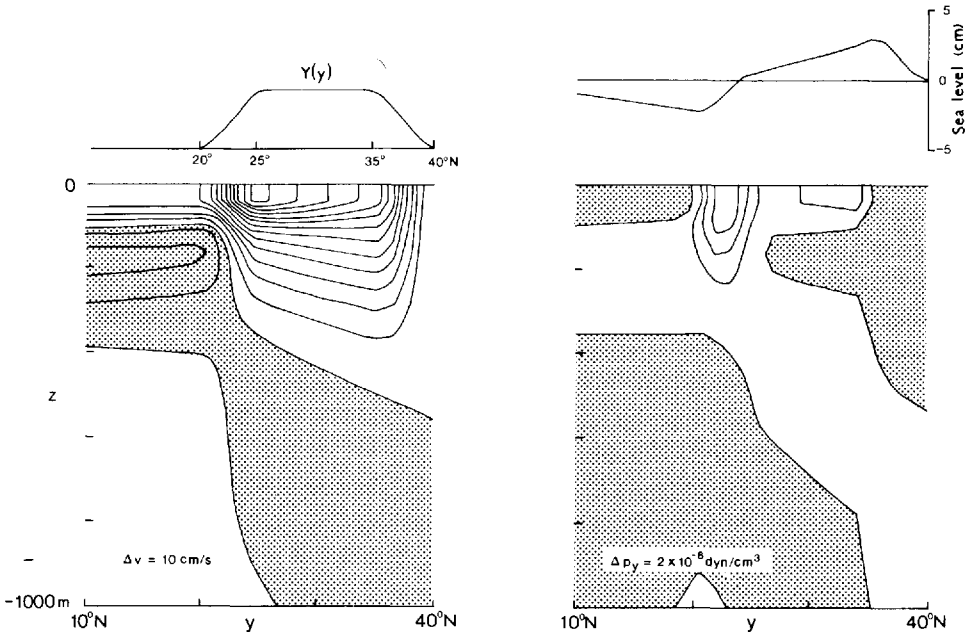

Figure 11. As in Figure 6, except driven by a northward wind with offshore curl. The contour interval for the alongshore pressure gradient is 2×10^{-8} dyn/cm^3. Figures 9 and 10 show zonal sections across this flow. Various aspects of the current are related to the structure of the forcing function in the lower right panel of Figure 8.

diffuse equatorward flow below 300 m at 25N, but no significant undercurrent there. An important, and at first surprising, result is that an appreciable undercurrent develops *south* of the wind patch. This undercurrent is shown in the zonal section at 10N (Fig. 10), and in the meridional section at $x = 8$ km (Fig. 11). This southward flow is caused by the strong onshore interior flow located at the southern edge of the wind (Fig. 8). Part of this onshore flow bends north, providing some of the water for the poleward current to the north, but the rest bends to the south.

Other features of the coastal solution are also related to the structure of the forcing function. Note in Figure 11 that in the region 25–35N the surface current strengthens toward the equator whereas the subsurface flow weakens (that is, subsurface v-contours tilt up toward the equator). The surface strengthening is due to the offshore Ekman flux that is present in this latitude band (the unshaded area shallower than 50 m along section BB in Fig. 8), just as in the curl-free solution. The subsurface weakening is forced by the weak, deep onshore flux that is proportional to β_y (the broad, shaded area from 50–500 m along section BB in Fig. 8).

Mathematically, the current structure south of the wind can be viewed as being the superposition of two coastal solutions: one solution is forced by offshore interior flow (the unshaded region along section BB in Fig. 8) and is associated with northward coastal currents; the other is forced by onshore flow (the shaded region along section BB in Fig. 8), and is associated with southward coastal currents. If the two solutions were identical in structure they would cancel south of the wind. It is the mismatch between them that allows the undercurrent to exist.

d. The model Somali Current. The above solutions use values for ν_h and a wind field that is typical for eastern-boundary models. These parameters are now set so that solutions are relevant to the Somali Current system. Horizontal diffusivity is increased to 10^7 cm/s, a commonly used value in models of western-boundary circulation. The wind field is chosen to resemble the observed wind in Figure 1b. The meridional profile extends from 5N to 20N as indicated above the right panel of Figure 12. Its zonal profile is constant in the range $0 \leq x \leq 500$ km and then drops smoothly to zero at $x =$ 1000 km with a cosine taper. Its amplitude is 4 dyn/cm^2, a value consistent with Figure 1b when the drag coefficient is .0014.

Figure 12 illustrates the resulting flow structure, showing a zonal section across the coastal current at 2N (left panel) and a meridional section along the current maxima at 44 km offshore (right panel). An undercurrent exists south of the wind, for the same dynamical reason as the one in Figures 10 and 11. The maximum speed of the undercurrent is 45 cm/s, that of the surface current is 160 cm/s, and the current width is about 75 km. These properties are all roughly in agreement with the observations discussed in the Introduction. Unfortunately we cannot investigate the fate of the coastal currents farther to the south, since the model breaks down near the equator.

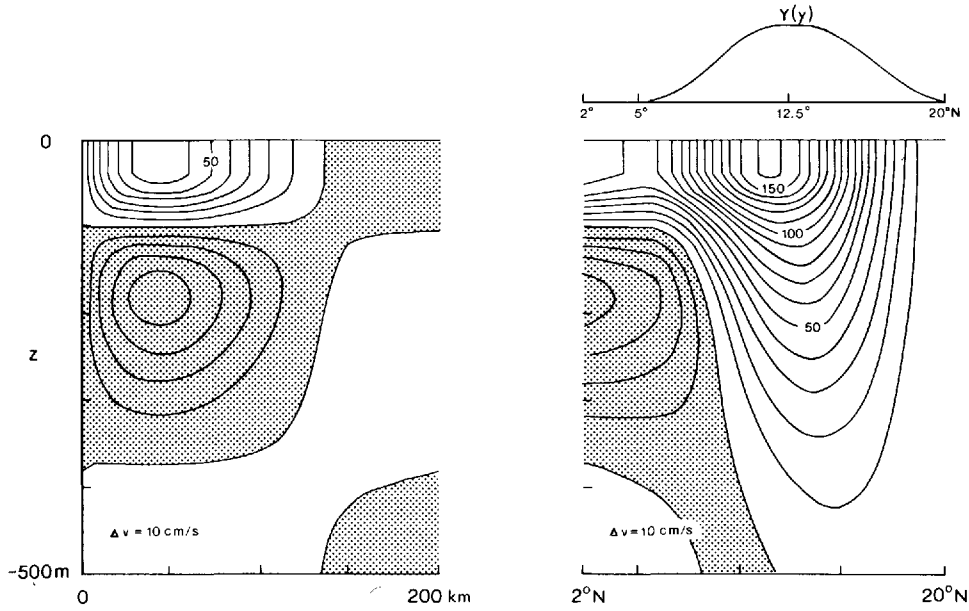

Figure 12. Zonal section at 2N (left panel) and meridional section at $x = 44$ km (right panel) of the alongshore flow field driven by a wind that resembles the observations in Figure 1b. The contour interval is 10 cm/s, and regions of southward flow are shaded. Diffusivities used are $\nu_{min} = 1$ cm^2/s and $\nu_h = 10^7$ cm^2/s. An undercurrent exists south of the region of the wind. The structure and strength of the current agrees roughly with observations off Somalia.

4. Summary and discussion

The eastern-boundary model of McCreary (1981) has been extended to apply to a western ocean boundary and to include wind curl. The model is linear, viscous, continuously stratified, flat-bottomed, and is driven only by the alongshore component of the wind.

Solutions are represented as expansions in vertical modes, and the dynamics of low-order and high-order modes differ considerably. For a few low-order modes ($n \gtrsim 5$–10), the interior circulation tends to be in Sverdrup balance and boundary currents have a structure similar to a Munk layer. These modes superpose to generate strong horizontal currents, but little coastal upwelling. For high-order modes, the interior circulation is in Ekman balance and the dynamics of boundary currents are two-dimensional. These modes superpose to generate Ekman flow offshore and significant coastal upwelling.

The alongshore flow driven by a curl-free wind band (Figs. 5–7) has a strong poleward surface current and *no* coastal undercurrent. This response differs markedly from that along the eastern boundary. The reason for this difference is that eastern-

boundary coastal currents associated with low-order modes leak offshore due to the β effect, and so the alongshore currents there are dominated by contributions from intermediate modes. At the western boundary this process cannot occur, and the low-order modes dominate the alongshore flow field. In contrast, the transverse circulations are very similar at both boundaries. The reason for this similarity is that the transverse circulations are affected most strongly by contributions from high-order modes, and these modes have the same response to the wind at both boundaries.

The unbounded solution forced by a wind patch of limited extent has features similar to a Sverdrup flow. For example, it has a surface circulation mainly confined to the edges of the wind patch (Fig. 8). Vertical mixing diffuses the circulation out of the mixed layer, and contour lines tilt downward to the west due to the presence of vertical mixing, in agreement with the solution in the Appendix.

The coastal flow forced by a wind having a negative offshore curl is more intense in the latitude band of the wind than that forced by a curl-free wind; in contrast, south of the wind the surface flow is weaker and there is an undercurrent (Figs. 9–12). The forcing function for this flow is the zonal flow shown in the lower right panel of Figure 8. The strong offshore flow near the northern edge of the wind forces poleward currents to the south. The onshore flow near the southern edge forces equatorward flow to the south, thereby weakening the poleward surface current and generating the undercurrent.

The appearance of the undercurrent south of the wind patch is consistent with several observations reviewed in the Introduction. They show that the Southwest Monsoon reaches a maximum at about 10–15N, and has a negative offshore curl. The observed undercurrent at 5N has a width scale of 50–100 km and a monthly mean speed of 20 cm/s, although the instantaneous speed may reach high values of the order of 60 cm/s. Our solution has a width scale of 75 km and a maximum speed of 45 cm/s.

This study is clearly only a step in the modelling of coastal circulation in upwelling regions along western boundaries. The solutions raise a number of interesting dynamical questions that need further study. For example, how does the coastal circulation respond to a seasonally varying wind? What are the coastal currents like at the equator? Is it possible to force significant cross-equatorial flow in a linear model? Does the coastal response change significantly if the western boundary has the structure of a realistic continental shelf, rather than a vertical barrier? What is the influence of nonlinearities on the subsurface currents? In addition, a thorough parameter study including realistic winds and basin geometry is obviously necessary to see if observed features along the Somali coast can be predicted accurately. We are currently beginning to work on several of these problems.

Acknowledgments. The work was supported by ONR Grant No. N00014-85-K-0019, and partially by NSF Grant No. ATM-82-05491. Computations were performed on the CRAY-1 computer at the National Center for Atmospheric Research. NCAR is supported by the

National Science Foundation. We are indebted to the late Walter Düing and to Fritz Schott, who first stimulated our interest in carrying out a modelling study of the Somali Current. We also thank Kevin Kohler for his programming assistance and Kathy Maxson for drafting the figures.

APPENDIX

Vertical structure

When there is no vertical mixing in the model, the circulation generated in the ocean interior tends to remain confined to the surface mixed layer. [See the discussion of Eqs. (11) and (25).] When mixing is included and there is wind curl, the currents extend into the deep ocean and develop an interesting vertical structure (Fig. 8). Because the solution (4) is represented as a superpositon of many vertical modes, it is not at all obvious why this structure develops. Stommel and Veronis (1957) found the response of an unbounded ocean to a zonally periodic wind without using an expansion into vertical modes, and the following discussion is an application of their approach to our model.

Consider the response of the model to a wind of the form $\tau^y = \tau_o \exp(ikx)$, where k is a positive number. Provided that N_b is constant, solutions to (1) have the form $\exp(ikx + imz)$ where m is a root of

$$\frac{\nu f^2}{N_b^2} m^4 + k^2(\nu + \nu_h f^2/N_b^2)m^2 + (\nu_h k^4 - ik\beta) = 0. \tag{A1}$$

[Equation (A1) can be obtained directly from (13) by the replacement $c_n \rightarrow N_b/m$.] We look for a solution that vanishes with depth and satisfies the two boundary conditions $\nu v_z = \nu ikp_z = \tau^y$ and $w = N_b^2(\nu p_{zzz} - \nu_h k^2 p_z) = 0$ at the ocean surface. The solution for the pressure field is

$$p = \frac{\tau^y/k\nu}{m_2^2 - m_1^2}\left[\frac{1}{m_2}\left(m_1^2 + \frac{\nu_h}{\nu}k^2\right)e^{im_2 z} - \frac{1}{m_1}\left(m_2^2 + \frac{\nu_h}{\nu}k^2\right)e^{im_1 z}\right]e^{ikx}, \tag{A2}$$

where m_1 and m_2 are the two roots of (A1) with negative imaginary parts.

For a large-scale wind field, large enough for the terms proportional to k^2 and k^4 to be negligible in (A1), the two appropriate roots are $m_1 = a \exp(-i\,7\pi/8)$ and $m_2 = a \exp(-i3\pi/8)$, where $a = (k\beta N^2/\nu f^2)$. It follows that for the exponential $\exp(im_1 z + ikx)$ lines of constant phase are vertical near the surface. The exponential $\exp(im_1 z)$ decays with depth more slowly than $\exp(im_2 z)$ does, and therefore dominates the response in the deeper ocean. Thus, in the deeper ocean lines of constant phase bend to tilt downward toward the west with a slope given by

$$s = \frac{k}{a\left|\cos\frac{7\pi}{8}\right|} = \left(\frac{\nu k^3 f^2}{\beta N_b}\right)^{1/4} \sec\frac{\pi}{8}. \tag{A3}$$

The unbounded solution in Figure 8 has a similar vertical structure, even though the wind field is not periodic; v-contours are oriented vertically near the ocean surface, but tilt westward at greater depths.

Note that it is only possible to satisfy two surface boundary conditions in writing down the solution (A2). This problem is due to the assumption of alongshore geostrophy, a restriction that filters Ekman layers out of the model. If the term νu_{zz} is not neglected, then the equation analogous to (A1) is eighth-order in m, the additional roots corresponding to Ekman layers at the ocean surface and bottom.

REFERENCES

Anderson, D. L. T. and D. W. Moore. 1979. Cross-equatorial inertial jets with special relevance to very remote forcing of the Somali Current. Deep-Sea Res., *26,* 1–22.

Anderson, D. L. T. and P. B. Rowlands. 1976. The Somali Current response to the southwest monsoon: the relative importance of local and remote forcing. J. Mar. Res., *34,* 395–417.

Brown, O. B., J. G. Bruce and R. H. Evans. 1980. Evolution of sea surface temperature in the Somali Basin during the southwest monsoon of 1979. Science, *209,* 595–597.

Cox, M. 1976. Equatorially trapped waves and the generation of the Somali Current. Deep-Sea Res., *23,* 1139–1152.

—— 1979. A numerical study of Somali Current eddies. J. Phys. Oceanogr., *9,* 311–326.

Düing, W., R. L. Molinari and J. C. Swallow. 1980. Somali Current: Evolution of surface current. Science, *209,* 588–590.

Knox, R. A. and D. L. T. Anderson. 1985. Recent advances in the study of the low-latitude ocean circulation. Prog. Oceanogr., *14,* 259–317.

Leetmaa, A., D. R. Quadfasel and D. Wilson. 1982. Development of flow field during the onset of the Somali Current, 1979. J. Phys. Oceanogr., *12,* 1325–1342.

Lin, L. B. and H. E. Hurlburt. 1981. Maximum simplification of nonlinear Somali Current dynamics, *in* Monsoon Dynamics, M. J. Lighthill and R. P. Pearce, eds., Cambridge University Press, 541–555.

Luther, M. E. and J. J. O'Brien. 1985. A model of the seasonal circulation in the Arabian Sea forced by observed winds. Prog. Oceanogr., *14,* 353–385.

McCreary, J. P. 1981. A linear stratified ocean model of the coastal undercurrent. Phil. Trans. Roy. Soc. Lond., *A302,* 385–413.

Munk, W. 1950. On the wind-driven ocean circulation. J. Meteorol., *7,* 79–93.

Philander, S. G. H. and P. Delecluse. 1983. Coastal currents in low latitudes (with application to the Somali and El Niño Currents). Deep-Sea Res., *30,* 887–902.

Quadfasel, D. R. and F. Schott. 1983. Southward subsurface flow below the Somali Current. J. Geophys. Res., *88,* 5973–5979.

Schott, F. 1983. Monsoon response of the Somali Current and associated upwelling. Prog. Oceanogr., *12,* 357–381.

Schott, F. and D. R. Quadfasel. 1982. Variability of the Somali Current system during the onset of the southwest monsoon, 1979. J. Phys. Oceanogr., *12,* 1343–1357.

Stommel, H. and G. Veronis. 1957. Steady convective motion in a horizontal layer of fluid heated uniformly from above and cooled non-uniformly from below. Tellus, *9,* 401–407.

Received: *10 January, 1985;* revised: *17 May, 1985.*